(Received 25 December 2025, Accepted 20 January 2026, Scheduled 9 February 2026)

Broadband Array Aperture Fill Time Correction Algorithm Based on Low-Complexity Variable Fractional Delay Filter

Yufan Wang[1], Mingwei Shen[2], Zixuan Wang[2], and Guodong Han[3,*]

[1] College of Information Science and Engineering, Hohai University, Changzhou 213200, Jiangsu, China
[2] College of Computer Science and Software Engineering, Hohai University, Nanjing 211100, Jiangsu, China
[3] The 54th Research Institute of CETC, Shijiazhuang 050081, Hebei, China

ABSTRACT: To address the aperture fill time problem in broadband arrays, this study proposes an efficient delay compensation algorithm based on a variable fractional delay (VFD) filter with high numerical stability. A low-complexity Newton structure was introduced into the VFD Lagrange interpolation algorithm, and the numerical stability was significantly enhanced by centrally offsetting the element delay parameters and avoiding the explicit inversion of the transformation matrix. Subsequently, the robust Newton-VFD was applied to the implementation of the broadband array aperture fill time correction algorithm. The algorithm utilizes a cascaded architecture consisting of coarse integer-delay compensation and fine fractional-delay correction via Newton-VFD. Simulation results demonstrate that the proposed low-complexity Newton-VFD significantly reduces hardware complexity while maintaining excellent magnitude-frequency characteristics, which enables efficient and high-precision correction of the broadband array aperture fill time.

1. INTRODUCTION

With the rapid evolution of modern communication and radar technologies, narrow-band arrays can no longer satisfy the requirements for information transmission rate, precision, and reliability, which has led to the widespread application of broadband arrays in fields, such as communication and radar. Because of the physical size of the antenna array, echo signals cannot arrive simultaneously at the receiving end, and the resulting aperture fill time has a non-negligible influence [1]. Particularly in array radar signal processing, the aperture fill time induces antenna beam pointing deviation, main-lobe broadening after pulse compression, and a reduction in effective bandwidth, thereby constraining radar performance. Therefore, aperture fill time [2] has emerged as a significant research direction in the field of modern array signal processing.

To address the issue of aperture fill time, researchers have proposed various methods that can be primarily categorized into time and frequency-domain approaches. Time-domain methods are fundamentally based on the True Time Delay (TTD) and include techniques such as delay lines and Fractional Delay Filters (FDF) [3]. Specifically, the implementation of FDFs mainly involves the window function method, Lagrange interpolation (LI) method [4], and Farrow structure-based [5] Variable Fractional Delay (VFD) filter. Frequency-domain methods primarily involve decomposing the broadband signal into narrowband sub-bands, correcting them individually via phase compensation, and recombining them to reconstruct the broadband signal [6].

This study focuses on an in-depth investigation of time-domain fractional delay filters [7]. Conventional fractional delay filters were designed for a pre-set fixed fractional delay value [8]. They relied on a fixed set of filter tap coefficients derived from a constant delay parameter. However, when the delay parameter changes, the entire filter must be redesigned and the coefficients reloaded, resulting in poor real-time performance and flexibility, as well as high memory resource consumption. In contrast, Variable Fractional Delay (VFD) filters effectively address these limitations [9]. Typically implemented using the Farrow structure, VFD filters express filter coefficients as polynomial functions of the delay parameter. By simply updating the parameter, new coefficients are generated, achieving the dynamic tunability of the delay. The Farrow structure is based on polynomial approximation [10, 11]. The Newton structure [12], proposed in recent years, is based on Newton's divided difference formula and can further reduce complexity through state-space diagonalization. However, it suffers from robustness issues. Therefore, this study aims to optimize computational efficiency and enhance system robustness while adopting a low-complexity Newton structure.

This study presents a novel aperture fill time correction algorithm based on a low-complexity Newton-VFD. By integrating Newton structure with Lagrange interpolation, the algorithm achieves a significant reduction in computational complexity. Furthermore, robustness is enhanced through delay parameter centralization and an optimization strategy that circumvents explicit matrix inversion, effectively overcoming the numerical instability issues associated with high-order filters. Finally, a cascaded processing architecture integrating integer delay correction and fractional delay compensation is established to re-

* Corresponding author: Guodong Han (hgd_cetc@163.com).

alize high-precision aperture fill time correction using the proposed Newton-VFD.

The remainder of this paper is organized as follows. Section 2 introduces the design of the Farrow structure filter based on the Lagrange interpolation algorithm. Section 3 derives the transformation matrix of the Farrow-Newton structure, centralizes the delay parameters, and optimizes the inversion of the transformation matrix to avoid numerical instability at high orders. Section 4 proposes a broadband array aperture fill time correction algorithm based on the designed low-complexity robust VFD. Section 5 presents the simulation verification of the optimized Newton fractional delay filter and its application to the aperture fill time correction of the array radar. Finally, the conclusions are presented in Section 6.

2. PRINCIPLE OF LI IN FARROW-VFD

The Lagrange interpolation method performs polynomial fitting in the time domain [13] by using the Lagrange basis function $h_k(d)$ to form a linear combination of discrete sample points. The expression for $h_k(d)$ is as follows:

$$h_k(d) = \prod_{\substack{m=0 \\ m\neq k}}^{N} \frac{d-m}{k-m}, \quad k = 0, 1, \ldots, N \tag{1}$$

where N represents the order of the filter; k represents the index of the k Lagrange basis function; d is the fractional delay parameter; and m is the integer index variable in the product operation.

The classical Tapped Delay Line (TDL) fractional delay filter requires the generation of distinct filter coefficients for varying delay values, which result in poor real-time performance. In contrast, the Farrow structure eliminates the need to recalculate the coefficient matrix when the delay parameter changes. The corresponding tap coefficients can be generated by substituting the updated delay parameters. Consequently, this structure effectively resolves the issue of real-time performance issues. The architecture of the Farrow filter is illustrated in Fig. 1, where the filter coefficient expression is expanded and represented in the form of a polynomial sum of d^m as follows:

$$h_k(d) = \sum_{m=0}^{M} c_m(k) \cdot d^m, \quad k = 0, 1, \ldots, N \tag{2}$$

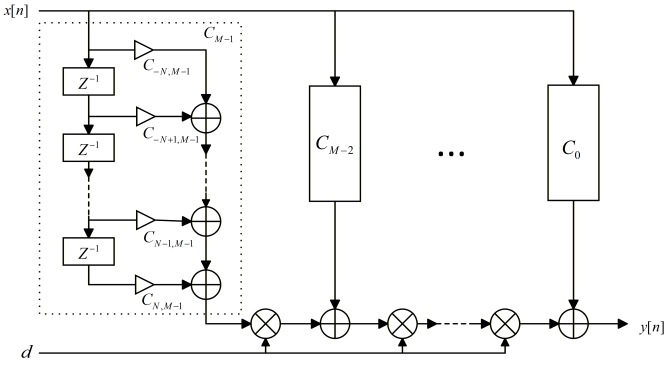

FIGURE 1. Block diagram of Farrow filter structure.

where $c_m(k)$ is the coefficient of the m-th polynomial at the k-th tap, and all $c_m(k)$ forms the coefficient matrix C. The transfer function of the filter is expressed as follows:

$$H_d(z) = \sum_{m=0}^{M} \left(\sum_{k=0}^{N} c_m(k) z^{-k} \right) d^m = \sum_{m=0}^{M} C_m(z) \cdot d^m \tag{3}$$

where M represents the number of filters, and N is the order of the sub-filters. Usually, let $M = N$.

3. IMPROVED LI IN NEWTON-VFD

3.1. Transformation Matrix for Newton-VFD

In contrast to the Farrow structure, the Newton structure [14] utilizes a forward difference operation mechanism, thereby avoiding complex calculations associated with high-order polynomials. Consequently, it demonstrates significant advantages in low-power scenarios or applications with stringent real-time requirements. This approach effectively reduces the computational load and substantially simplifies the complexity of the hardware implementation. Its structure is illustrated in Fig. 2.

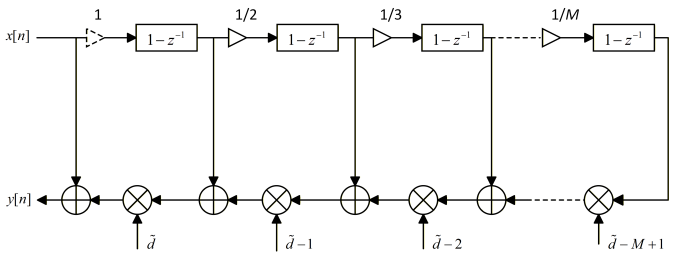

FIGURE 2. Block diagram of Newton filter structure.

This study aims to represent the transfer functions of Farrow and Newton structures in vector form and to derive the transformation formula between them. The conversion from the Farrow structure to the Newton structure was achieved using the transformation matrix.

Transforming formula (3) into matrix form gives the Farrow transfer function as:

$$H_{\text{Farrow}}(\mathbf{z}, \mathbf{D}) = \mathbf{D}^{\mathrm{T}} \mathbf{C} \mathbf{z} \tag{4}$$

where the delay vector $\mathbf{D} = [1, d, d^2, d^3, \ldots, d^N]^{\mathrm{T}}$ of the Farrow structure; d is the delay parameter of the Farrow structure; the discrete time domain $\mathbf{z} = [1, z^{-1}, z^{-2}, \ldots, z^{-N}]^{\mathrm{T}}$, and the two are power-basis vectors.

Define the delay parameter $\tilde{d} = d - \frac{N}{2}$ of the Newton structure. According to Fig. 2, the transfer function of the Newton structure is defined as follows:

$$H_{\text{Newton}}(\tilde{\mathbf{z}}, \tilde{\mathbf{D}}) = \tilde{\mathbf{D}}^{\mathrm{T}} \tilde{\mathbf{C}} \tilde{\mathbf{z}} \tag{5}$$

where the delay vectors $\tilde{\mathbf{D}} = [1, \tilde{d}(\tilde{d}-1), \tilde{d}(\tilde{d}-1)(\tilde{d}-2), \ldots, \tilde{d}(\tilde{d}-1), \ldots, (\tilde{d}-N+1)]$ of the Newton structure and the discrete time domain $\tilde{\mathbf{z}} = [1, 1-z^{-1}, (1-z^{-1})^2, \ldots, (1-z^{-1})^N]^{\mathrm{T}}$ are the basis vectors of the difference quotient.

To convert the delayed-domain power basis $\mathbf{D}$ to the divided-difference basis $\tilde{\mathbf{D}}$ of the Newton structure, which transforms the Farrow transfer function into Newton form, the binomial

coefficient matrix $\mathbf{T}_{d\_0}$ and Stirling number matrix $\mathbf{T}_{d\_1}$ are defined. Both $\mathbf{T}_{d\_0}$ and $\mathbf{T}_{d\_1}$ are lower triangular matrices.

The elements of $\mathbf{T}_{d\_0}$ are constructed using binomial coefficients and the delay offset $-\frac{N}{2}$, and the general formula is as follows:

$$\mathbf{T}_{d\_0}[k][i] = \binom{k}{i}\left(-\frac{N}{2}\right)^{k-i}, \quad 0 \le i \le k \le N \tag{6}$$

where $\binom{k}{i}$ denotes a binomial coefficient, which represents the number of ways to partition k elements into i circular permutations. $(-\frac{N}{2})^{k-i}$ is the power term of the delay offset. Taking $N = 4$ as an example, $\mathbf{T}_{d\_0}$ is expressed by the following matrix:

$$\mathbf{T}_{d\_0} = \begin{bmatrix} 1 & 0 & 0 & 0 & 0 \\ -2 & 1 & 0 & 0 & 0 \\ 4 & -4 & 1 & 0 & 0 \\ -8 & 12 & -6 & 1 & 0 \\ 16 & -32 & 24 & -8 & 1 \end{bmatrix} \tag{7}$$

The elements of $\mathbf{T}_{d\_1}$ are constructed from the first type of unsigned Stirling number $\begin{bmatrix} k \\ i \end{bmatrix}$, and its general formula is as follows:

$$\mathbf{T}_{d\_1}[k][i] = (-1)^{k-i}\begin{bmatrix} k \\ i \end{bmatrix}, \quad 0 \le i \le k \le N \tag{8}$$

where $(-1)^{k-i}$ is a symbol correction term. Taking $N = 4$ as an example, $\mathbf{T}_{d\_1}$ is expressed as the following matrix:

$$\mathbf{T}_{d\_1} = \begin{bmatrix} 1 & 0 & 0 & 0 & 0 \\ 0 & 1 & 0 & 0 & 0 \\ 0 & -1 & 1 & 0 & 0 \\ 0 & 2 & -3 & 1 & 0 \\ 0 & -6 & 11 & -6 & 1 \end{bmatrix} \tag{9}$$

Therefore, the delay domain transformation matrix $\mathbf{T}_d = \mathbf{T}_{d\_0} \cdot \mathbf{T}_{d\_1}$ is defined, where $\mathbf{T}_d[k][i]$ is the sum of the products of the corresponding elements in the k-th row of $\mathbf{T}_{d\_1}$ and the i-th column of $\mathbf{T}_{d\_0}$, as shown in the following formula:

$$\begin{aligned} \mathbf{T}_d[k][i] &= \sum_{m=i}^{k} \mathbf{T}_{d\_1}[k][m] \cdot \mathbf{T}_{d\_0}[m][i] \\ &= \sum_{m=i}^{k}\left[(-1)^{k-m}\begin{bmatrix} k \\ m \end{bmatrix}\right] \cdot \left[\binom{m}{i}\left(-\frac{N}{2}\right)^{m-i}\right] \end{aligned} \tag{10}$$

To achieve mapping from the discrete-time domain power basis $\mathbf{z}$ to the difference quotient basis $\tilde{\mathbf{z}}$ of the Newton structure, the discrete-time domain transformation matrix $\mathbf{T}_z$ is defined, and its general formula is as follows:

$$\mathbf{T}_z[k][m] = (-1)^{k-m}\binom{k}{m}, \quad 0 \le m \le k \le N \tag{11}$$

Therefore, $\mathbf{T}_z$ can be expressed as the following matrix when $N = 4$:

$$\mathbf{T}_z = \begin{bmatrix} 1 & 0 & 0 & 0 & 0 \\ 1 & -1 & 0 & 0 & 0 \\ 1 & -2 & 1 & 0 & 0 \\ 1 & -3 & 3 & -1 & 0 \\ 1 & -4 & 6 & -4 & 1 \end{bmatrix} \tag{12}$$

Moreover, the difference quotient basis satisfies $\tilde{\mathbf{D}} = \mathbf{T}_d \cdot \mathbf{D}$, and the discrete difference quotient basis satisfies $\tilde{\mathbf{z}} = \mathbf{T}_z \cdot \mathbf{z}$. Therefore, the Newton transfer function can be derived from the Farrow transfer function through the following matrix transformation:

$$\begin{aligned} H_{\text{Farrow}}(\mathbf{z}, \mathbf{D}) &= \mathbf{D}^{\mathrm{T}}\mathbf{C}\mathbf{z} = \mathbf{D}^{\mathrm{T}}\left(\mathbf{T}_d\mathbf{T}_d^{-\mathrm{T}}\right)\mathbf{C}\left(\mathbf{T}_z^{-1}\mathbf{T}_z\right)\mathbf{z} \\ &= \left(\mathbf{T}_d\mathbf{D}\right)^{\mathrm{T}}\left(\mathbf{T}_d^{-\mathrm{T}}\mathbf{C}\mathbf{T}_z^{-1}\right)\left(\mathbf{T}_z\mathbf{z}\right) \\ &= \tilde{\mathbf{D}}^{\mathrm{T}}\tilde{\mathbf{C}}\tilde{\mathbf{z}} = H_{\text{Newton}}(\tilde{\mathbf{z}}, \tilde{\mathbf{D}}) \end{aligned} \tag{13}$$

where the filter coefficients of the Newton structure satisfy $\tilde{\mathbf{C}} = \mathbf{T}_d^{-\mathrm{T}}\mathbf{C}\mathbf{T}_z^{-1}$.

As demonstrated by the proof, the Farrow structure can be transformed into a Newton structure via a transformation matrix, and the transfer functions of both structures are completely equivalent. Consequently, given this equivalence, when prioritizing filter robustness, the Farrow structure can be converted into a Newton structure. By leveraging the reduced ill-conditioning of the Newton structure matrix operations, the issue of numerical instability in high-order designs is mitigated, thereby enhancing the robust performance of variable fractional delay filtering.

3.2. Robustness Optimization of High-Order LI in Newton-VFD

The Lagrange interpolation algorithm suffers from numerical instability under high-order scenarios. With increasing order, the condition number of the coefficient matrix deteriorates, and the ill-conditioning intensifies, leading to significant errors during the inversion of the transformation matrix. Therefore, to enhance the robustness of the filter in high-order applications, this study optimizes the Lagrange interpolation-based Newton-VFD algorithm through a two-fold approach.

First, the time parameter centralization of the Lagrange interpolation method was studied. Ref. [15] utilized the convolution method to avoid explicit inversion and split the Lagrange interpolation function expression into two parts: denominator and numerator. The formula is as follows:

$$h_m(d) = \prod_{\substack{i=0, \\ i\neq m}}^{N} \frac{d-i}{m-i} = \lambda_m P_m(d) \tag{14}$$

where λ_m is the normalized coefficient.

For the molecular part $P_m(d) = \prod_{\substack{i=0, \\ i\neq m}}^{N}(d-i)$, let the delay parameter $d = \frac{N}{2} + \tilde{d}$ and transform the Lagrange interpolation polynomial from a polynomial related to d to one related to $\tilde{d}$. Through mathematical reconstruction, numerical defects

are avoided, and at the same time, coefficient symmetry is constructed to make the polynomial coefficients more stable as the order N increases. The formula is as follows:

$$P_m(d) = Q_m(\tilde{d}) = \prod_{\substack{i=0,\\ i\neq m}}^{N} \left(\frac{N}{2} + \tilde{d} - i\right) \tag{15}$$

when N is an even number and $m \neq \frac{N}{2}$, let $i = \frac{N}{2} + i'$, and simplified $Q_m(\tilde{d})$ can be obtained as follows:

$$Q_m(\tilde{d}) = \prod_{\substack{i'=-N/2,\\ i'\neq m-N/2}}^{N/2} (\tilde{d} - i') \tag{16}$$

Furthermore, during the conversion from the Farrow structure to the Newton structure, the inverse operation of transformation matrices such as $\mathbf{T}_{d\_0}$, $\mathbf{T}_{d\_1}$, and $\mathbf{T}_z$ is crucial. The traditional explicit inversion method has a high computational complexity. Therefore, this study adopts a method to avoid the explicit inversion of the transformation matrix involved when converting a Farrow structure to a Newton structure.

Let $\mathbf{T}_{d\_0}$ be an $N+1$-order lower triangular matrix that satisfies the diagonal element $T_{ii} = \pm 1$, and the symbols of the non-diagonal elements are uniform. For any lower triangular matrix, the inverse matrix remains a lower triangular matrix. Therefore, the diagonal elements of the inverse matrix $\mathbf{T}_{d\_0}^{-1}$ are:

$$(\mathbf{T}_{d\_0}^{-1})[i][i] = \frac{1}{\mathbf{T}_{d\_0}[i][i]} = \mathbf{T}_{d\_0}[i][i] \tag{17}$$

The non-diagonal elements of $\mathbf{T}_{d\_0}^{-1}$ can be obtained through the recursive formula:

$$(\mathbf{T}_{d\_0}^{-1})[i][j] = -\frac{1}{\mathbf{T}_{d\_0}[i][i]} \sum_{k=j}^{i-1} \mathbf{T}_{d\_0}[i][k] \cdot (\mathbf{T}_{d\_0}^{-1})[k][j] \tag{18}$$

Because the non-diagonal symbols of $\mathbf{T}_{d\_0}$ are uniform, the non-diagonal element symbols of $\mathbf{T}_{d\_0}^{-1}$ are consistent with those of $\mathbf{T}_{d\_0}$. Therefore, the absolute values of the elements in $\mathbf{T}_{d\_0}^{-1}$ and $\mathbf{T}_{d\_0}$ are exactly the same and can be simplified as follows:

$$\mathbf{T}_{d\_0}^{-1} = \text{abs}(\mathbf{T}_{d\_0}) \tag{19}$$

$\mathbf{T}_{d\_1}$ is the sign correction matrix of the first type of Stirling number, and its elements are defined by formula (8). The first type of Stirling number matrix $\mathbf{S}$ and second type of Stirling number matrix $\mathbf{S}_{\text{inv}}$ satisfy the orthogonal relationship $\mathbf{S} \cdot \mathbf{S}_{\text{inv}} = \mathbf{I}$, from which $\mathbf{S}_{\text{inv}} = \mathbf{S}^{-1}$ can be obtained. The specific relationship is as follows:

$$\sum_{m=i}^{j} \begin{bmatrix} j \\ m \end{bmatrix} \begin{Bmatrix} m \\ i \end{Bmatrix} = \delta_{ij} \tag{20}$$

where δ_{ij} is the Kronecker function.

After the symbolic correction of $\mathbf{T}_{d\_1}$, its inverse matrix can be represented by the symbolic correction form of the second type of Stirling number:

$$(\mathbf{T}_{d\_1}^{-1})[k][i] = (-1)^{k-i} \begin{Bmatrix} k \\ i \end{Bmatrix} \tag{21}$$

Because all Stirling numbers are non-negative integers, and $(-1)^{k-i}$ have the same sign pattern in $\mathbf{T}_{d\_1}$ and $\mathbf{T}_{d\_0}^{-1}$, the absolute value form of $\mathbf{T}_{d\_0}^{-1}$ is equivalent to the second type of Stirling number matrix:

$$\mathbf{T}_{d\_1}^{-1} = \text{abs}(\mathbf{S}_{\text{inv}}) \tag{22}$$

where $\mathbf{S}_{\text{inv}}$ is the sign correction matrix of the second type of Stirling numbers.

The transformation matrix $\mathbf{T}_d^{-T}$ can be calculated by $\mathbf{T}_{d\_0}^{-1}$ and $\mathbf{T}_{d\_1}^{-1}$

$$\mathbf{T}_d^{-T} = (\mathbf{T}_{d\_0}^{-1} * \mathbf{T}_{d\_1}^{-1})^T \tag{23}$$

The elements of $\mathbf{T}_z$ are defined in formula (11), and the elements of $\mathbf{T}_z^2$ are calculated as follows:

$$\left(\mathbf{T}_z^2\right)[k][i] = \sum_{m=i}^{k} \mathbf{T}_z[k][m] \cdot \mathbf{T}_z[m][i] \tag{24}$$

Substituting the properties of the binomial coefficients in formula (24), the following can be obtained:

$$\sum_{m=i}^{k} \binom{k}{m} \binom{m}{i} (-1)^{k-m} (-1)^{m-i} = \delta_{ki} \tag{25}$$

It can be proven that $\mathbf{T}_z^2 = I$, that is, $\mathbf{T}_z$ conforms to the characteristics of a pair matrix, and its inverse matrix satisfies the following equation:

$$\mathbf{T}_z^{-1} = \mathbf{T}_z \tag{26}$$

The above-mentioned inverse matrix transform makes use of the consistency of the lower triangular sign, orthogonality of the Stirling number, and self-inverse transformation of the connection matrix. This avoids the high computational load of the general inverse transformation and effectively prevents the numerical instability problem that occurs during the inverse transformation of the transformation matrix.

The Newton structural coefficient matrix corresponding to the Lagrange Farrow structural coefficient $\mathbf{C}$ is $\tilde{\mathbf{C}} = \mathbf{T}_d^{-\mathrm{T}} \mathbf{C} \mathbf{T}_z^{-1}$. Its matrix form at $N = 4$ is expressed as:

$$\tilde{\mathbf{C}} = \mathbf{T}_d^{-\mathrm{T}} \mathbf{C} \mathbf{T}_z^{-1} = \begin{bmatrix} 1 & -4 & 6 & -4 & 1 \\ 0 & -1 & 4 & -6 & 4 \\ 0 & 0 & \frac{1}{2} & -2 & 3 \\ 0 & 0 & 0 & -\frac{1}{6} & \frac{2}{3} \\ 0 & 0 & 0 & 0 & \frac{1}{24} \end{bmatrix} \tag{27}$$

In summary, this study derives the coefficient matrix transformation formulation from the Lagrange-based Farrow structure to the Newton structure and verifies their functional equivalence in variable fractional delay filtering. Furthermore, the

numerical stability of the algorithm was significantly enhanced by employing delay parameter centralization and avoiding explicit matrix inversion.

4. APERTURE FILL TIME CORRECTION ALGORITHM BASED ON NEWTON-VFD

The physical dimensions of the antenna array will introduce the aperture fill time. In broadband systems, it is specifically manifested as beam skew and pulse broadening phenomena. To mitigate these impairments effectively, a robust and efficient delay compensation scheme is essential. Building on Section 3, this section proposes a practical correction architecture centered on the designed low-complexity, robust Newton-VFD filter. This optimized structure ensures stable amplitude-frequency characteristics while significantly reducing hardware costs. Consequently, integrating this filter into a cascaded "integer-to-fractional" architecture achieves high-precision aperture fill time correction, along with optimal resource utilization.

In this study, an isotropic Uniform Linear Array (ULA) was adopted as the signal receiving array model [16], as shown in Fig. 3. The ULA consists of M array elements with an inter-element spacing of l. It is assumed that a far-field plane wave signal $s(t)$ impinges on the ULA at a specific angle θ.

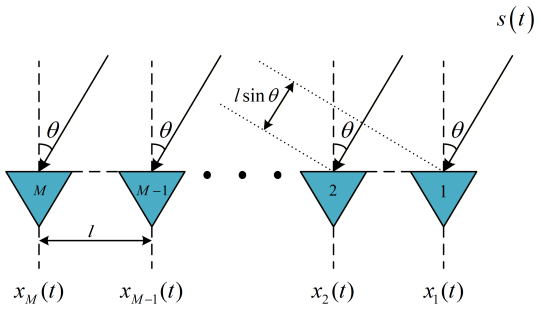

FIGURE 3. ULA receiving array model.

According to the M-element array shown in Fig. 3, the path difference between the received signals of two adjacent elements is $l\sin(\theta)$. Taking the rightmost element as the reference and given the speed of light $c = 3 \times 10^8$, the propagation delay of the received signal at the m-th element is:

$$\tau_m = (m-1)l\sin\theta/c, \quad m = 1, 2, \ldots, M \tag{28}$$

Therefore, the received signal at the m-th array element is:

$$x_m(t) = x(t - \tau_m) \tag{29}$$

Owing to the influence of the broadband array geometry [17], the received signals at the remaining array elements have varying degrees of delay compared to the reference element. To ensure that the signals received by all array elements can be synchronized, enabling accurate and undistorted signal synthesis during spatial processing such as beamforming, and to precisely estimate the azimuth angle of the signal source, aperture fill correction must be performed. The correction process is illustrated in Fig. 4.

Let τ_m denote the propagation delay of the received signal at the m-th array element. Upon digitization at a sampling frequency f_s, the corresponding discrete delay D_m is typically a non-integer, necessitating fractional delay compensation. To address this, we propose a cascaded architecture based on delay decomposition, in which the delay of each element is separated into integer and fractional components and processed sequentially.

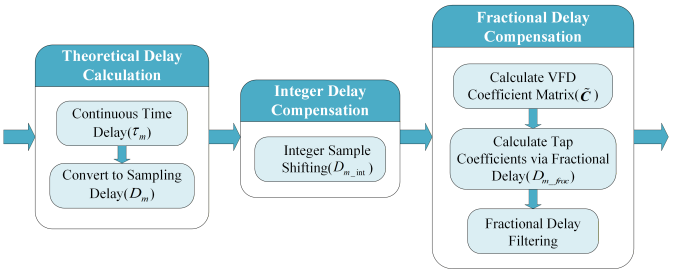

FIGURE 4. Flowchart of the aperture fill time correction algorithm.

$$\begin{aligned} D_m &= \tau_m \cdot f_s \\ D_{m\_\text{int}} &= \text{floor}(D_m) \\ D_{m\_\text{frac}} &= D_m - D_{m\_\text{int}} \end{aligned} \tag{30}$$

Specifically, regarding the integer delay component D_{m_int}, coarse correction is performed using integer sample shifting. For the fractional delay component D_{m_frac}, precise correction is achieved by first computing the coefficient matrix based on the Newton-VFD, and subsequently deriving the corresponding filter tap coefficients according to the specific fractional delay value.

5. SIMULATION RESULTS AND ANALYSIS

This section presents a model simulation analysis based on the theoretical derivations in the preceding sections. First, it verifies the performance equivalence between the Farrow and Newton structures achieved using the transformation matrix. Second, to address the issue of numerical instability in high-order scenarios, it evaluates whether the combination of delay parameter centralization and avoidance of explicit transformation matrix inversion effectively enhances system robustness.

The simulation initially compared the Lagrange interpolation method with the cubic spline interpolation algorithm, as shown in Fig. 5. The results demonstrate that the Lagrange method exhibits superior amplitude-frequency characteristics, more precise fitting accuracy, higher passband flatness, and a closer approximation to the ideal frequency response. Consequently, all the subsequent simulation analyses in this study were based on the Lagrange interpolation method.

In the simulation, with the order set to $N = 4$, the amplitude-frequency characteristic curves are plotted for both the Lagrange interpolation-based Farrow fractional delay filter and the optimized Newton structure fractional delay filter. A comparison of these curves verifies the previously derived conclusion that the equivalence between the Farrow and Newton structures can be achieved using a transformation matrix. This provides experimental support for the convertibility of the two structures from the perspective of the frequency domain characteristics.

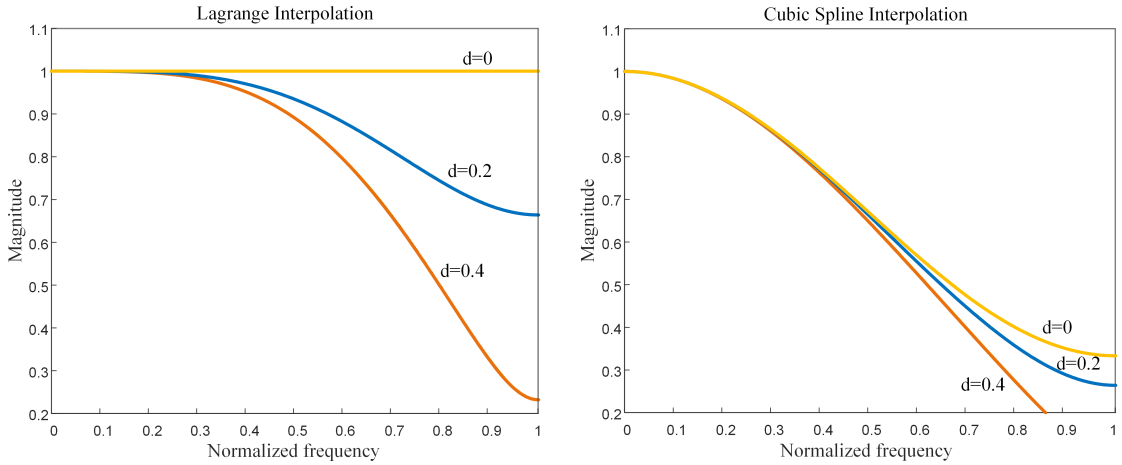

FIGURE 5. Comparison of interpolation algorithms.

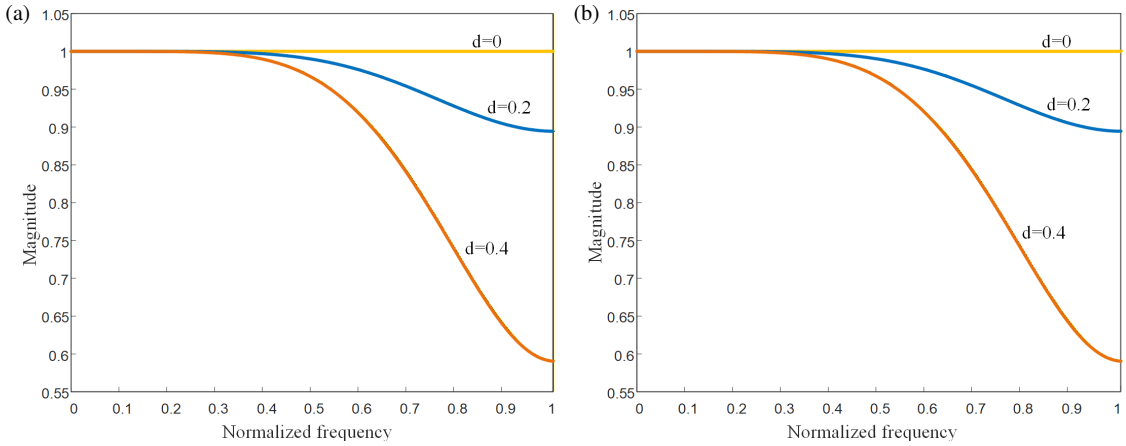

FIGURE 6. VFD amplitude-frequency characteristic curves with different structures. (a) Farrow structure. (b) Newton structure.

Figure 6 shows that the Farrow and Newton structures can achieve fully equivalent filtering results with the help of the transformation matrix. However, when $N > 14$, the coefficient matrix of the Lagrange interpolation method itself will have a catastrophic cancellation problem at a higher order, and the transformation matrix will be accompanied by numerical instability and accuracy loss problems. These factors jointly lead to significant ill-conditioned matrix problem in the Newton structure. Taking $N = 18$ and $N = 22$ as examples, as shown in Fig. 7, the amplitude-frequency characteristic curves are clearly displayed. At this point, the numerical instability problem of the fractional delay filter has become prominent, and the fractional delay function cannot be precisely realized.

To solve the above numerical instability problem, based on the original method, the delay parameter of the fractional delay filter is centralized, and the explicit inversion of the transformation matrix is avoided by combining the formula derivation, which improves numerical instability to a certain extent. After optimization, as shown in Fig. 8, the amplitude-frequency characteristic curves of the filter performed well when $N = 18$ and $N = 22$.

Figure 9 shows the magnitude response of Newton-VFD under different delay parameters when $N = 20$. From the image, it can be seen that the amplitude response surface within the effective passband shows extremely high flatness, proving that the Newton-VFD proposed in this study not only has a lower complexity but also maintains excellent passband characteristics and numerical stability.

Table 1 compares the condition numbers of the transformation matrices $\mathbf{T}_u$, $\mathbf{T}_z$ and the sum under different filter orders N, as well as the errors of the traditional method and the method proposed in this paper compared to the ideal filter. From Table 1, it can be seen that the condition number of the transformation matrix increases rapidly with the increase in order.

TABLE 1. Robustness index.

N	Cond ($\mathbf{T}_u$)	Cond ($\mathbf{T}_z$)	Error of traditional methods	Error of this article
4	1.91×10^4	9×10^1	7.88×10^{-15}	4.44×10^{-16}
18	5.57×10^{40}	1.21×10^{10}	5.27×10^{-2}	1.52×10^{-6}
22	2.65×10^{53}	2.79×10^{12}	6.93×10^{2}	1.00×10^{-2}

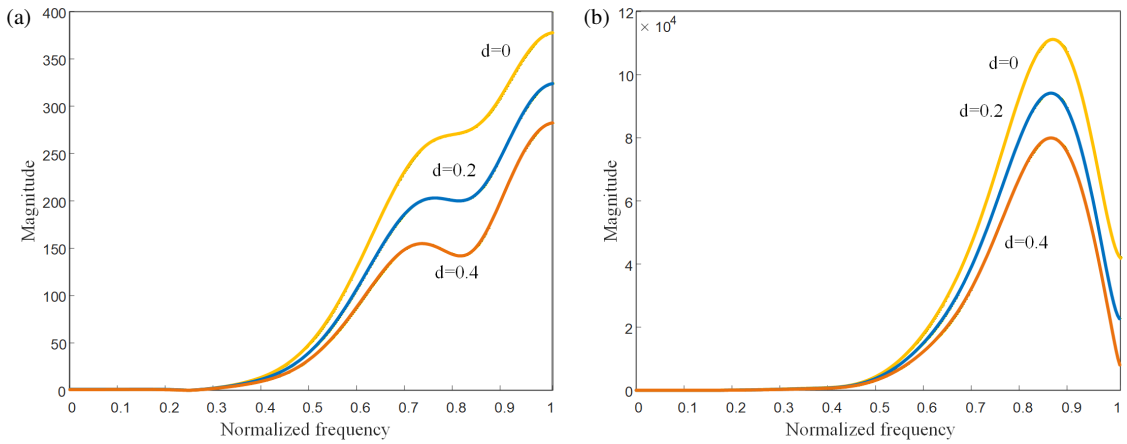

FIGURE 7. Amplitude-frequency characteristic curves of the nonrobust algorithm. (a) $N = 18$. (b) $N = 22$.

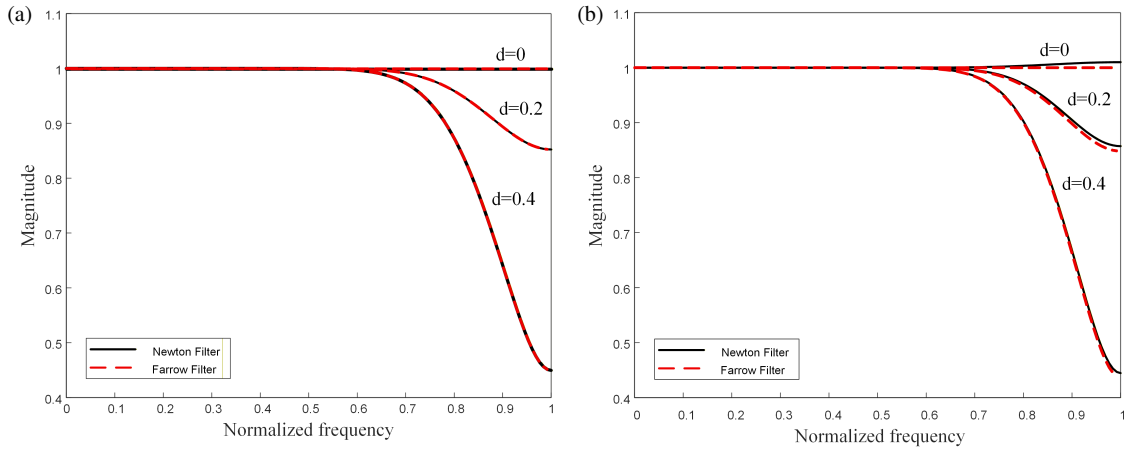

FIGURE 8. The amplitude-frequency characteristic curves after robust optimization. (a) $N = 18$. (b) $N = 22$.

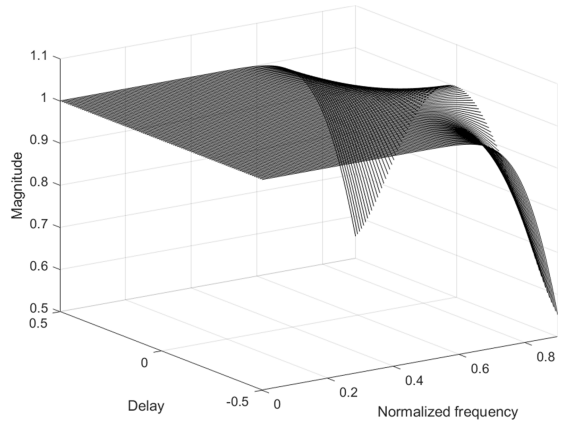

FIGURE 9. 3D magnitude response plot.

Due to the presence of ill-conditioned characteristics, the traditional method relying on explicit matrix inversion generates catastrophic numerical errors. In contrast, even at $N = 22$, the method proposed in this paper can still keep the error at a relatively low level, thereby demonstrating the excellent robustness of the Newton-VFD proposed in this paper.

Building upon the performance analysis and optimization of the Newton-VFD, this study further validates the engineering implementation of the filter for aperture fill time correction in broadband array radars. Assume that the number of array elements is $M = 32$, taking the 1st, 16th, and 31st elements as array elements as examples for plotting. As shown in Fig. 10, with the 1st element serving as the reference, the echo signals of the 16th and 31st elements exhibited varying degrees of time delay. As illustrated in Fig. 11, the aperture fill time effect became more pronounced following the range pulse compression of the received signals. The peak echo energy for distinct elements is distributed across different range cells, thereby manifesting the aperture fill time phenomenon.

To address the issue of delays caused by non-integer sampling periods encountered in the simulation, the broadband array aperture fill time correction algorithm based on the low-complexity robust VFD, proposed in the preceding section, is employed. A quantitative analysis of the delay parameters during the correction process is shown in Fig. 12. The blue trace depicts the initial delay values of the individual array elements, exhibiting a linearly increasing trend, consistent with the array wavefront arrival model. The red trace indicates the residual fractional delays that remain after integer compensation. Finally, the green trace demonstrates that the delay values for all

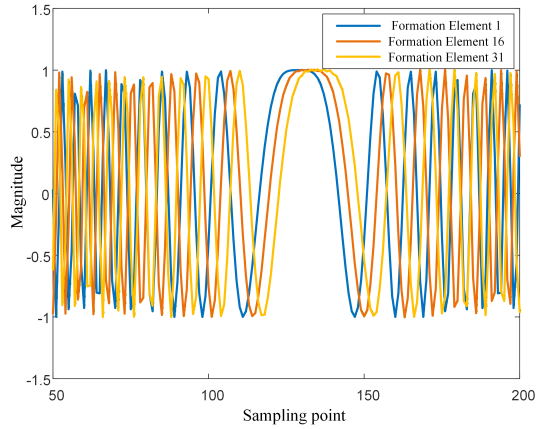

FIGURE 10. Raw echo signal.

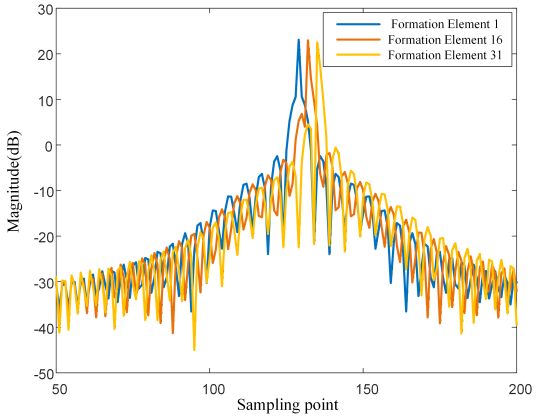

FIGURE 11. Echo signal after pulse compression.

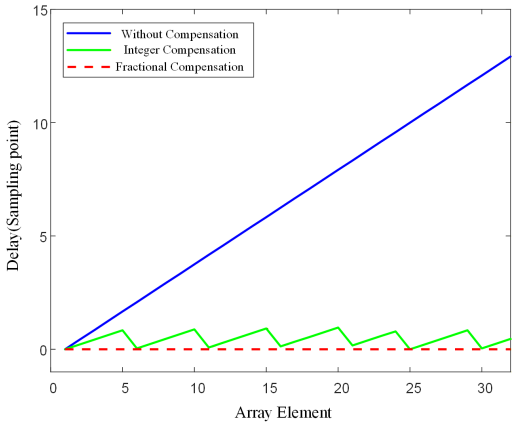

FIGURE 12. Raw echo signal.

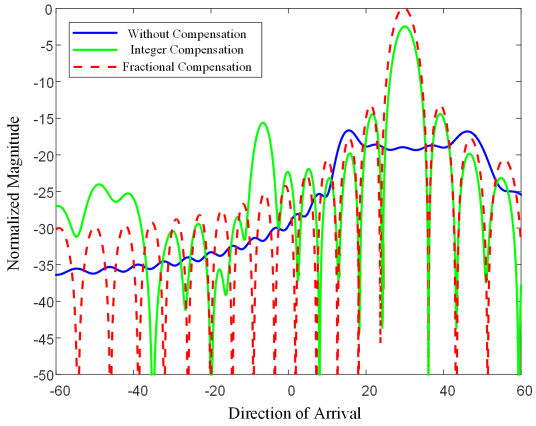

FIGURE 13. Array beam pattern.

the array elements were reduced to zero, thereby confirming the completeness of the correction process.

According to the two-stage aperture fill time correction algorithm proposed in this study, integer sample shifting is first performed to address the integer delay component, as depicted in Fig. 14. Compared to Fig. 11, the echo signals following integer delay compensation have achieved coarse correction; however, minor delay errors persist, corresponding to the red trace representing the fractional delay in Fig. 12. Consequently, the experiment was conducted to correct the fractional delay component. The resulting corrected echo signals are shown in Fig. 15, where the echo energy is more precisely concentrated within the same cell range. At this stage, the delay magnitude corresponds to the zero-out green trace shown in Fig. 12. Thus, the aperture fill time correction was completed, providing an optimized signal foundation for subsequent beamforming and parameter estimation.

Figure 13 shows the beam patterns in three states: without correction, integer delay correction, and fractional delay correction. The main lobe of the uncorrected beam is severely broadened, and the amplitude attenuation is severe. Through quantitative analysis of Fig. 13, it can be seen that the uncorrected wideband beam has a serious pointing deviation. When the simulation sets the target direction to 30°, the actual pointing is 15.6°, with an error of 14.4°. After the Newton-VFD correction proposed in this study, the beam points to 30.0°. At the same time, the peak side-lobe ratio (PSLR) was calculated in the simulation. Due to the defocusing effect of the uncorrected beam, the side-lobe level is high, and the PSLR is -3.54 dB. At this time, the interference suppression ability is poor, which will lead to false alarms in actual radar applications. In contrast, after the Newton-VFD correction, the PSLR improves to -13.23 dB, demonstrating the superiority of the algorithm in suppressing side lobes.

The experiment analyzed and compared the hardware complexity of VFD. Because the coefficient matrix $\tilde{\mathbf{C}}$ in the Newton structure exhibits the characteristic form of an upper triangular matrix, it significantly reduces the usage of adders and multipliers compared with the Farrow structure. This effectively enhances the overall operational efficiency and resource utilization of the system. Table 2 provides a comparison of adder and multiplier usage for $N = 18$ and $N = 22$.

The simulation implementation validates robust processing optimized through parameter centralization and matrix inversion. This demonstrates that, while maintaining equivalence with the Farrow structure, the Newton structure significantly reduces the computational complexity and conserves computational resources.

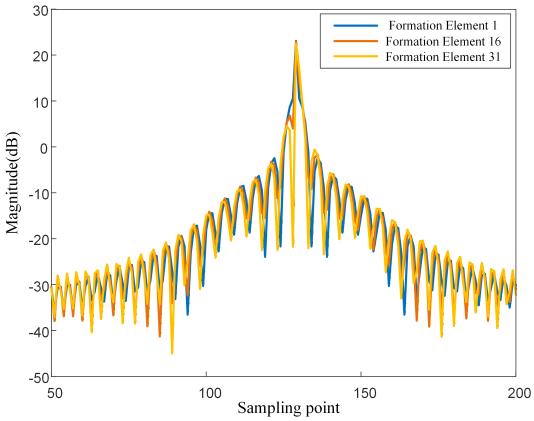

FIGURE 14. Integer delay compensation of the echo signal.

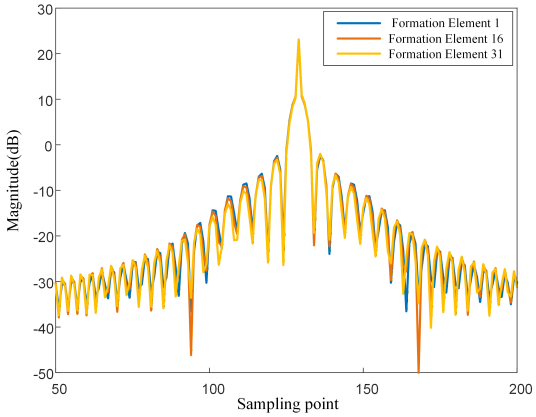

FIGURE 15. Fractional delay compensation of the echo signal.

TABLE 2. Hardware complexity.

	Farrow		Newton	
N	Add	Mult	Add	Mult
18	333	352	189	208
22	459	482	275	298

6. CONCLUSION

To address the aperture fill time in broadband array radar and its efficient, high-precision correction, this study investigates a correction algorithm based on a low-complexity robust Variable Fractional Delay (VFD) filter. This study prioritized the design of a low-complexity robust fractional delay filter based on a Newton structure. Specifically, to address the issues of computational complexity and numerical stability encountered by VFD filters in high-order applications, a robust low-complexity architecture was proposed. The Newton forward difference mechanism is introduced into the Lagrange interpolation type VFD to replace the traditional Farrow structure. By implementing delay parameter centralization and optimizing the transformation matrix inversion process, the Lagrange interpolation-based Newton structure VFD was enhanced. The delay parameters were shifted to the center of the interpolation interval, and the Lagrange interpolation polynomial was reconstructed, which alleviated the problem of the divergence of high-order polynomial coefficients. This optimization improves the system's robustness while simultaneously reducing the computational complexity. Furthermore, the mapping relationship between the geometric positions of array elements and delay parameters was established. It has constructed a comprehensive cascaded correction architecture, achieving coarse compensation through integer sampling shifting, and then performing fine correction on the remaining fractional delay using an optimized Newton-VFD. Future research could further explore the extended application of alternative interpolation algorithms and optimize the filter design architecture. By balancing computational complexity, system robustness, and practical feasibility, such work aims to provide more efficient and precise solutions for real-time signal processing systems.

REFERENCES

[1] Wang, J., D.-D. Cai, and F. Yang, "Aperture effect influence and analysis of wideband phased array radar," *Procedia Engineering*, Vol. 29, 1298–1303, 2012.

[2] Zhu, X. and K. Zhang, "A study on compensation of aperture fill time based on frequency-shifting," in *IET International Radar Conference 2013*, C0239, 2013.

[3] Canese, L., G. C. Cardarilli, L. D. Nunzio, R. Fazzolari, D. Giardino, M. Re, and S. Spanò, "Efficient digital implementation of a multirate-based variable fractional delay filter for wideband beamforming," *IEEE Transactions on Circuits and Systems II: Express Briefs*, Vol. 70, No. 6, 2231–2235, 2023.

[4] Tassart, S. and P. Depalle, "Analytical approximations of fractional delays: Lagrange interpolators and allpass filters," in *1997 IEEE International Conference on Acoustics, Speech, and Signal Processing*, Vol. 1, 455–458, Munich, Germany, 1997.

[5] Bakholdin, N., V. Chernienko, and S. Bakhurin, "Digital resampler based on farrow filter," in *2025 27th International Conference on Digital Signal Processing and its Applications (DSPA)*, 1–7, Moscow, Russian Federation, 2025.

[6] Huang, Y.-D., S.-C. Pei, and J.-J. Shyu, "WLS design of variable fractional-delay FIR filters using coefficient relationship," *IEEE Transactions on Circuits and Systems II: Express Briefs*, Vol. 56, No. 3, 220–224, 2009.

[7] Farrow, C. W., "A continuously variable digital delay element," in *IEEE International Symposium on Circuits and Systems*, Vol. 3, 2641–2645, Espoo, Finland, 1988.

[8] Duan, H., B. P. Ng, C. M. S. See, and J. Fang, "Broadband beamforming using TDL-form IIR filters," *IEEE Transactions on Signal Processing*, Vol. 55, No. 3, 990–1002, 2007.

[9] Zhou, W., M. Xu, and M. Shen, "A novel variable fractional delay filter design with sparsity within and across groups for wideband beamforming," *Remote Sensing Letters*, Vol. 16, No. 10, 1046–1056, 2025.

[10] Johansson, H. and O. Gustafsson, "Linear-phase FIR interpolation, decimation, and mth-band filters utilizing the Farrow structure," *IEEE Transactions on Circuits and Systems I: Regular Papers*, Vol. 52, No. 10, 2197–2207, 2005.

[11] Abbas, M., O. Gustafsson, and H. Johansson, "On the fixed-point implementation of fractional-delay filters based on the Farrow structure," *IEEE Transactions on Circuits and Systems I: Regular Papers*, Vol. 60, No. 4, 926–937, 2013.

[12] Sandhya, G., S. K. R, and B. T. S, "Design of low complexity arbitrary pass-band filter hardware using newton structure-based

lagrange interpolators," in *2022 IEEE 3rd Global Conference for Advancement in Technology (GCAT)*, 1–6, Bangalore, India, 2022.

[13] Deng, T.-B., "Coefficient-symmetries for implementing arbitrary-order lagrange-type variable fractional-delay digital filters," *IEEE Transactions on Signal Processing*, Vol. 55, No. 8, 4078–4090, 2007.

[14] Lamb, D., L. F. O. Chamon, and V. H. Nascimento, "Efficient filtering structure for spline interpolation and decimation," *Electronics Letters*, Vol. 52, No. 1, 39–41, 2016.

[15] Deng, T.-B., "Robust structure transformation for causal lagrange-type variable fractional-delay filters," *IEEE Transactions on Circuits and Systems I: Regular Papers*, Vol. 56, No. 8, 1681–1688, 2009.

[16] Wang, Y., L. Zhuang, and Y. Wang, "Influence of aperture fill time of wideband interference on anti-jamming method of multi-channel SAR," in *IET International Radar Conference (IRC 2023)*, 1022–1027, Chongqing, China, 2023.

[17] Zhou, W., M. Shen, D. Wu, and D. Zhu, "Efficient beam-scanning wideband sparse array synthesis with minimum element spacing control," *Signal Processing*, Vol. 238, 110194, 2026.